Rare Metal Materials and Engineering
Volume
Available online at **www.rmme.ac.cn**

Science Press

Cite this article as: Rare Metal Materials and Engineering,

ARTICLE

https://doi.org/10.12442/j.issn.1002-185X.20250595

Process Optimization for Preparing Uniform and Dense Tungsten Coatings on Throat Liners by CVD

Xie Zheng[1], Wang Longlong[1], Tan Chengwen[1,2], Yu Xiaodong[1,2], Ning Xianjin[1]

[1]School of Materials Science and Engineering, Beijing Institute of Technology, Beijing 100081, China; [2] Highpure Precision Materials (Suzhou) Co., Ltd., Suzhou 215211, China

Abstract: Tungsten's distinctive physical and chemical properties make it a highly suitable material for rocket applications. Chemical vapor deposition (CVD) is a promising technique for applying uniform tungsten coatings to complex-shaped components (e.g., rocket engine throat liner). This study adapts a previously established low-pressure CVD model for tungsten, enabling its application under atmospheric pressure conditions to deposit high-performance coatings on rocket engine throat liners. We investigate the influence of three distinct reactor configurations—a straight-tube inlet, an integrated gas distribution device, and a combination of a distribution device with a flow guide baffle—on the reactor's flow dynamics, thermal field, species concentration, and deposition kinetics. Numerical and experimental results demonstrate that the configuration incorporating both a distribution device and a baffle eliminates vortices within the liner region by promoting radial gas diffusion, thereby significantly improving flow field uniformity. This optimized design not only improves the uniformity of the deposition rate on the throat insert, but also slightly enhances the utilization efficiency of tungsten hexafluoride. This work provides a theoretical foundation for designing CVD systems for highly uniform tungsten coatings and offers a practical solution for their engineering application.

Key words: CVD; Tungsten; CFD; Fluent

1 Introduction

Tungsten, which possesses the highest melting point (≈ 3410 ℃) of all metals, exhibits exceptional physicochemical properties[1, 2]. These include high thermal conductivity (173 W/(m • K)), a low coefficient of thermal expansion, outstanding high-temperature strength, and excellent ablation resistance[3-7]. These characteristics make tungsten highly attractive for rocket applications. Notwithstanding these advantages, its high density (19.35 g/cm³) and poor machinability severely restrict its direct use[8]. A feasible strategy to circumvent these limitations is the application of tungsten coatings onto light-weight substrates. This approach effectively reduces component density while conferring the superior properties of tungsten to the composite system.

Among the techniques for depositing such coatings, physical vapor deposition (PVD), low-pressure chemical vapor deposition (LPCVD), and atmospheric pressure chemical vapor deposition (APCVD) are widely employed[9-13].

Tungsten coatings prepared by PVD are relatively thin, exhibit poor uniformity and inadequate step coverage, and are significantly constrained by the size and shape of the substrate. In addition, the low deposition rate restricts this technique primarily to the fabrication of nano-to micro-scale thin films, rendering such coatings unsuitable for harsh service conditions involving high temperatures and strong erosion.

In contrast, CVD enables the production of tungsten coatings with high purity and density, minimal surface defects, excellent uniformity, and strong adhesion to the

Received date:
Foundation item:
Corresponding author: Tan Chengwen, Ph.D.,Professor,School of Materials Science and Engineering, Beijing Institute of Technology, Beijing 100081, China, E-mail: tanchengwen@bit.edu.cn;Yu Xiaodong, Ph.D., Professor, School of Materials Science and Engineering, Beijing Institute of Technology, Beijing 100081, China, E-mail: yuxd@bit.edu.cn.

substrate, making it well-suited for complex-shaped cavity components. Moreover, compared with LPCVD, APCVD affords a higher deposition rate for tungsten coatings, providing a distinct ad-vantage for the preparation of throat liner coatings[12, 14, 15].

The CVD process is highly controllable, permitting precise adjustment of operational parameters—such as temperature, pressure, and gas flow rate—as well as modification of the reactor geometry to meet diverse application requirements. Ex-tensive research has been devoted to understanding tungsten growth mechanisms in CVD systems. For in-stance, Bryant[16] determined the activation energy for tungsten deposition via hydrogen reduction of WF_6 to be 67.0 kJ/mol under low-pressure conditions. Subsequently, Pauleau and Lami[11] established that the deposition rate depends on the partial pressures of the reactants, reporting reaction orders of zero with respect to WF_6 and one-half with respect to H_2 at relatively low pressure. They also correlated the loss of reaction selectivity with an increase in the partial pressure of HF. Building on previous research, Lakhotkin[17, 18] performed a rigorous chemical analysis of the H_2/WF_6 reduction system, concluding that CVD tungsten is primarily formed via the disproportionation reaction of tungsten subfluorides (e.g., WF_4).

Numerical simulation has become an indispensable methodology for investigating the CVD of tungsten, complementing experimental studies by enabling the prediction of key parameters such as species concentrations, pressure distributions, and deposition rates within the reactor. The foundation for such modeling was established by Arora and Pollard[19], who developed a detailed mechanistic framework for the H_2 reduction of WF_6 using statistical mechanics and transition state theory. Building on this, Kleijn et al[20]. refined this model and implemented it within the PHOENICS computational fluid dynamics software, facilitating the optimization of thin-film deposition processes. Raumann[21-23] et al. developed a model for tungsten-fiber-reinforced tungsten (W_f/W) composites and used this model to propose new deposition rate equations. These equations allow the calculation of partial pressures in CVD reactors and facilitate the modeling of reactions for W_f/W composites, thus enabling the prediction of interfacial contact conditions and potential pore formation on tungsten substrates. Using their CFD-optimized process parameters, they successfully synthesized dense Wf/W composites at a H_2:WF_6 flow ratio of 12.5:1. Furthermore, they simulated tungsten synthesis using the commercial software COMSOL Multiphysics and experimentally validated the model's accuracy. Raumann et al. also systematically investigated the dependence of the deposition rate on the partial pressure of WF_6, ultimately proposing a new rate equation that incorporates modified semi-empirical constants. Wang Y et al[24]. used ANSYS Fluent to simulate the CVD tungsten deposition process and adopted an orthogonal experimental design to optimize process parameters, thereby identifying the optimal parameter combination for simultaneously maximizing the deposition rate and coating uniformity.

Although extensive research has been conducted on tungsten deposition via CVD， the vast majority of existing studies focus on elucidating the fundamental reaction mechanisms of tungsten CVD and formulating empirical deposition rate equations. Yet systematic investigations into the structural optimization of CVD reactors tailored specifically for com-plex-shaped components remain scarce. Achieving a uniform, dense tungsten coating on rocket engine throat liners—a typical representative of such complex-shaped hot-end components—remains a formidable technical challenge, as their intricate profiled geometry induces severe local inhomogeneities in gas flow distribution, thermal field, and reactant diffusion paths at the substrate surface. This imposes stringent requirements for the precise regulation of gas-phase parameters (e.g., precursor concentration, flow velocity, and pressure distribution) at the coating-substrate interface, which is essential to avoid critical coating defects including nonuniform thickness, poor compactness, and low deposition efficiency. Notably, the coupling effects of reactor structure on the flow field, thermal field, and precursor concentration field—the core factors governing coating uniformity for irregular substrates—have not been fully explored or quantitatively characterized to date. To address this critical research gap and overcome the corresponding engineering bottleneck, this study innovatively employs Computational Fluid Dynamics (CFD) to conduct a

coupled multi-physical field analysis, integrating flow field, thermal field, species concentration field, and deposition kinetics, for an APCVD reactor dedicated to rocket engine throat liners. We systematically investigate and optimize three distinct reactor inlet configurations, and subsequently validate the reliability of the numerical simulation results through controlled deposition experiments. For experimental validation, high-purity tungsten hexafluoride (WF_6, 99.999%) and hydrogen (H_2, 99.999%) are used as precursor gases to fabricate high-performance tungsten coatings on throat liner substrates under atmospheric pressure conditions, with the ultimate objective of developing a structurally optimized APCVD reactor that enables the deposition of uniform, dense tungsten coatings on complex-shaped aerospace components.

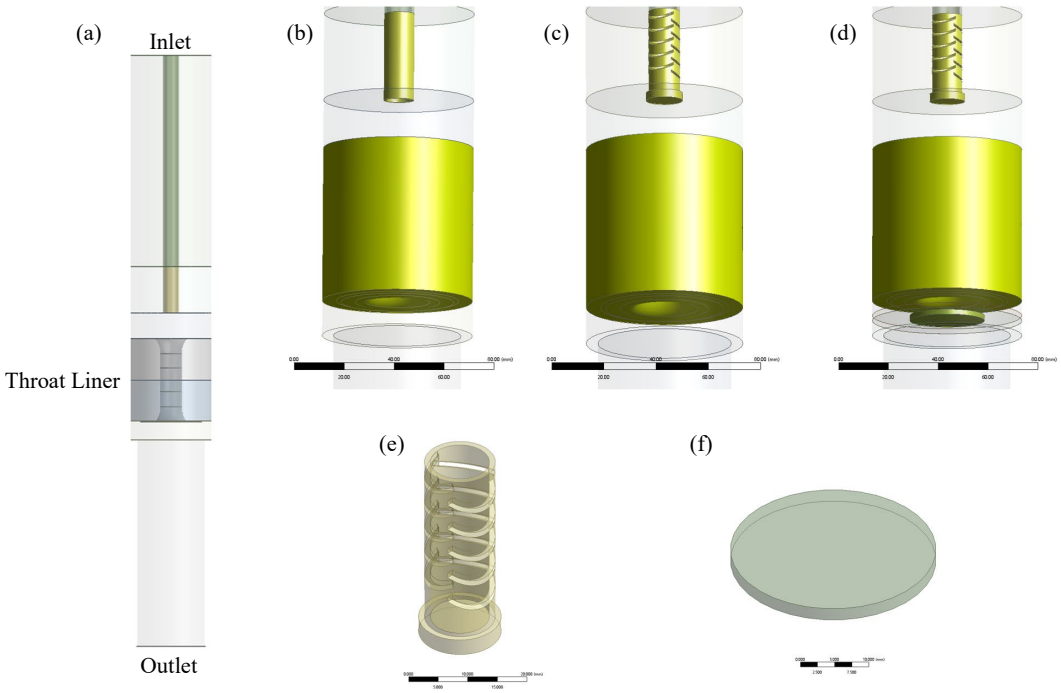

Figure1. Structures of the Deposition Chamber

(a) Deposition chamber with a straight-tube gas inlet;(b) Important part of the deposition chamber with a straight-tube gas inlet;(c) Important part of the deposition chamber with a gas distribution device;(d) Important part of the deposition chamber with both a gas distribution device and a flow baffle;(e) Three-dimensional structure of the gas distribution device;(f) Three-dimensional structure of the flow baffle

2 Experiment Method

2.1 Numerical Method

The deposition process via the hydrogen reduction of tungsten hexafluoride (WF_6) can be divided into three consecutive kinetic stages:(1) Mass transport: It involves the diffusion of H_2 and WF_6 toward the substrate surface and the escape of HF from the reaction zone, and its rate is predominantly determined by hydrodynamic parameters (e.g., Reynolds number, Schmidt number).(2) Boundary layer diffusion: It involves the transfer of reactants (H_2, WF_6) and products (tungsten, HF) across the boundary layer.(3) Surface reaction: It comprises the adsorption of reactant molecules on the substrate surface, heterogeneous surface chemical reactions, and the desorption of reaction products, and its rate is governed by surface chemical kinetics.

To simplify the numerical model, the following assumptions are adopted for the deposition process: (1) The deposition process is approximated as a single-step reaction.(2) The effect of substrate surface roughness on boundary layer mass transfer is neglected.(3) Kinetic effects related to surface adsorption and desorption processes are neglected. Although these simplifying assumptions may compromise the model accuracy, they significantly enhance computational efficiency while preserving the key features of the main physical phenomena.

2.1.1 Geometric model and mesh generation.

To improve process efficiency and tungsten hexafluoride (WF_6) utilization, this study deposits tungsten coatings on two liners simultaneously, laying the foundation for large-scale coating deposition on multiple liners.

The CVD reactor system for tungsten coating preparation mainly comprises a gas inlet device and a cylindrical reaction chamber, where the main deposition reactions occur. As shown in Figure 1, the deposition chamber has three configurations: (a) Deposition chamber with a straight-tube gas inlet; (b) Important part of the deposition chamber with a straight-tube gas inlet;(c) Important part of the deposition chamber with a gas distribution device;(d) Important part of the deposition chamber with both a gas distribution device and a flow baffle; Figures 2 (e) and 2 (f)specifically show three-dimensional structural diagrams of the gas distribution device and the flow baffle, respectively. Existing research results have shown that the gas distribution device can improve the gas flow distribution in the reaction chamber, which mainly achieves its function by dispersing a single large gas flow into multiple small gas flows. The flow guide plate can guide the gas flow to flow along the wall surface, avoiding the occurrence of eddy current phenomenon of the gas flow in the deposition chamber.

To optimize computational accuracy and efficiency, a differentiated mesh generation strategy is used for different regions: the hexahedral meshes are applied to the upper and lower flow field regions of the throat liner, while locally refined tetrahedral meshes are used for the complex structural areas of the reaction chamber adjacent to the throat liner. Addition-ally, boundary layers are incorporated in the region near the throat liner wall to ensure the accuracy of computational results. Figure 2 shows the mesh generation of the deposition chamber, where: (a) Cross-sectional mesh on the XY-plane; (b) Mesh along the Y-direction; (c) Mesh near the throat liner; (d) Mesh of a partial region of the throat liner.

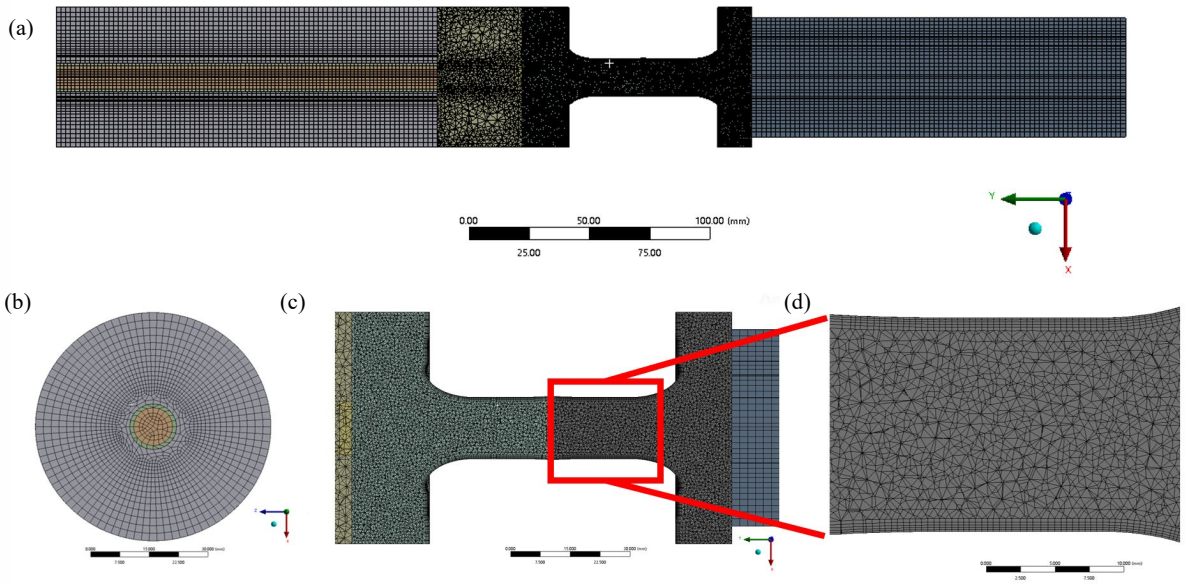

Figure2. the mesh generation of the deposition chamber

(a) Cross-sectional mesh on the XY-plane;(b) Mesh along the Y-direction;

(c) Mesh near the throat liner;(d) Mesh of a partial region of the throat liner

2.1.2 Boundary Conditions.

The boundary conditions considered in this study include the following: flow velocity, pressure, temperature, and heat transfer coefficient at the inlet, outlet, and various wall surfaces (i.e., interfaces involving mass and energy exchange). These boundary conditions are determined using historical empirical values and calculations based on the corresponding specific experimental parameters. The flow rate of H_2 is 2.2 standard liters per minute, and that of WF_6 is 10 g/min. The heating temperature is 560°C (833 K).

2.2 Experimental Methodology

Figure 3 schematically illustrates the experimental setup for the CVD of tungsten. The deposition process was conducted at a pressure slightly above atmospheric to prevent air ingress, which would oxidize contaminants and compromise coating quality. Mass flow metes provided precise regulation of the gas flow rates. The outlet of the deposition chamber was connected to a tail gas treatment system, where reaction by-products such as HF were neutralized by a saturated calcium hydroxide ($Ca(OH)_2$) solution, enabling the safe disposal of the tail gas.

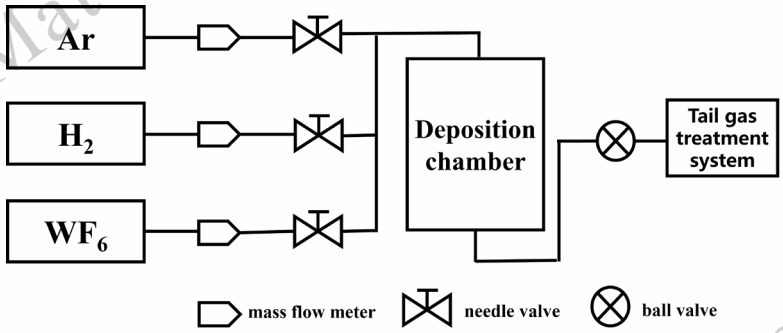

Figure 3. Schematic Diagram of the Experimental Setup for CVD Tungsten Coating Deposition

3. Result and discussion

3.1 Influence of Different Structures on Gas Velocity Field

Owing to its axisymmetric geometry, we can observe the two-dimensional cross-sectional condition of the deposition chamber to analyze the entire chamber. Figure 4 presents the simulated velocity distributions for the three reactor configurations:(a)straight-tube inlet,(b)integrated gas distribution device, and(c) combination of a distribution device and a flow baffle. In all cases, the constricted geometry of the throat liner induces a pronounced flow acceleration, as evidenced by the increased velocity magnitudes within the liner section.

In the straight-tube inlet configuration (Figure 4a), the main gas flow is directed axially into the liner cavity, resulting in significant velocity in homogeneity above the throat liner. Analysis of the local flow field reveals that the liner's contoured geometry induces localized vortices near the inlet, which disrupts the uniform distribution of reactants. The integration of a gas distribution device (Figure 4b) addresses this issue by altering the gas introduction to a gradual lateral flow. This mode prevents direct impingement, promotes controlled gas accumulation above the liner, and effectively suppresses vortex formation. However, in this configuration, gas exiting the liner cavity flows directly downward, depleting reactant concentration at the trailing end of the throat liner and adversely affecting the reaction kinetics. This limitation is mitigated by the addition of a flow baffle (Figure 4c). In this optimized design, the gas exiting the liner is redirected radially outward, maintaining higher reactant concentrations in the bilateral regions and thereby promoting a uniform tungsten deposition rate across the entire liner surface. The resulting stable and uniform flow distribution significantly enhances deposition efficiency and coating quality, ultimately yielding a more uniform and denser tungsten coating.

3.2 Influence of Different Structures on the Temperature Field

Figure 5 presents the temperature distributions for the three reactor configurations, corresponding to the flow fields analyzed in Figure 5:(a) straight-tube inlet, (b) integrated gas distribution device, and (c) combination of a distribution device and a flow baffle.

Analysis indicates a uniform surface temperature within the liner cavity across all three configurations. The temperature in the upper fluid region and along the cold walls progressively decreases from the central heating zone toward the chamber ends. In contrast, the lower fluid region maintains a stable thermal profile. This stability is attributed to the fact that the gas leaving the liner cavity is sufficiently heated to 800 K, resulting in the minimized thermal gradient in the lower chamber section.

In the straight-tube configuration (Figure 5a), the straight-tube gas inlet causes the reactive gases to not be sufficiently preheated, leading to a decrease in the internal temperature of the throat liner. This suboptimal temperature can hinder the kinetics of the tungsten dep-

osition reaction, ultimately compromising coating quality. In contrast, the configurations employing gas distribution devices (Figures 5b and 5c) alter the gas inlet methodology, allowing for sufficient preheating of the reactant gases prior to their entry into the liner. This enhanced thermal homogenization elevates the cavity temperature to near-optimal levels, thereby improving deposition efficiency and yielding tungsten coatings with superior uniformity and density.

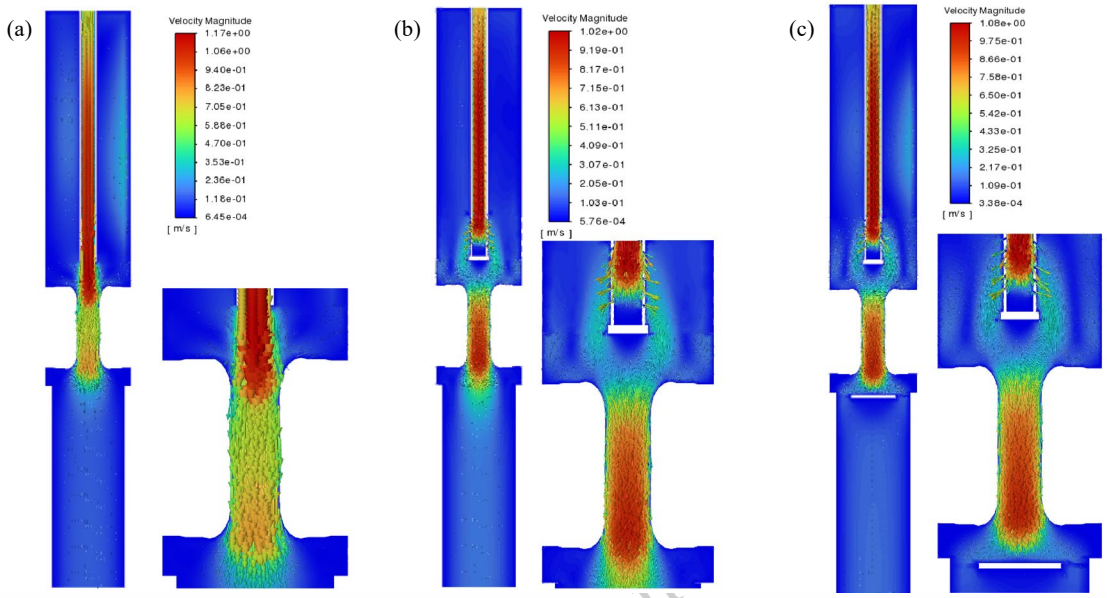

Figure 4. Velocity Contour Plots in the Three Types of Deposition Chambers

(a) Velocity contour plot of the straight-tube inlet deposition chamber; (b) Velocity contour plot of the deposition chamber with a gas distribution device; (c) Velocity contour plot of the deposition chamber with both a gas distribution device and a flow baffle

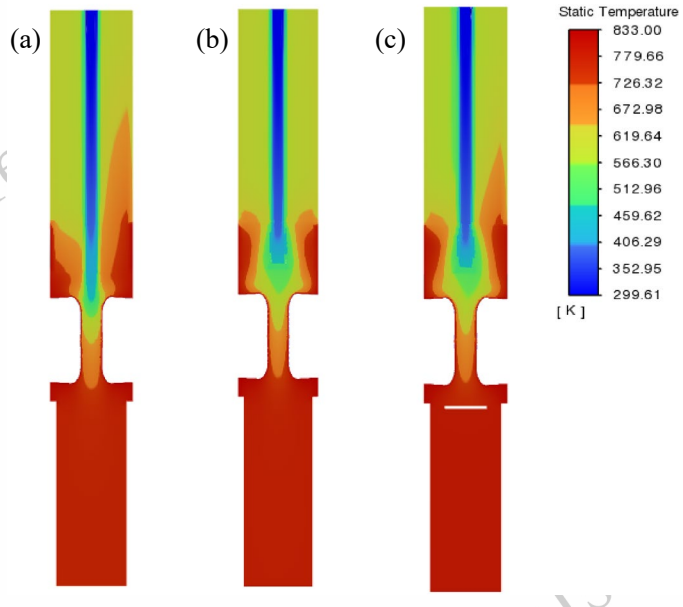

Figure 5. Temperature Contour Plots of Deposition Chambers with Different Structures

(a) Tem-perature contour plot of the straight-tube inlet deposition chamber; (b) Temperature contour plot of the deposition chamber with a gas distribution device; (c) Temperature contour plot of the deposition chamber with both a gas distribution device and a flow baffle

3.3 Influence of Different Structures on Gas Concentration Field

Figures 6 and 7 present the mole fraction distributions of H_2 and WF_6, respectively, for the three chamber configurations. A comparative analysis reveals that the dis-

tinct structural designs significantly influence the concentration profiles of both precursor gases. Figure 6 details the hydrogen mole fraction for the (a) straight-tube inlet, (b) integrated gas distribution device, and (c) combined device with flow baffle configurations.

In the straight-tube configuration (Figure 6a), the direct injection of gas into the liner cavity, coupled with vortex formation above it, results in a significantly higher hydrogen mole fraction inside the inlet tube than in the surrounding region. This pronounced in-homogeneity adversely affects the uniformity of the vapor deposition reaction rate. As shown in Figures 6b and 6c, the incorporation of a gas distribution device shifts the inlet mode from axial to lateral introduction. This change enhances the uniformity of the hydrogen distribution and suppresses vortex formation. However, in the configuration with only the distribution device (Figure 6b), the downward flow of gas exiting the liner cavity depletes the hydrogen mole fraction near the base, consequently reducing the local deposition rate. This limitation is resolved in the final configuration (Figure 6c), where a flow baffle redirects the effluent gas laterally. This prevents the depletion of hydrogen at the liner base, ensuring a more consistent reactant concentration and deposition rate.

The mole fraction distribution of the primary reactant, WF_6, generally correlates with that of H_2. Given the high cost of WF_6, its utilization efficiency is a critical metric for reactor performance. Across all configurations, the WF_6 mole fraction is high-est at the inlet and diminishes toward the outlet. In both the straight-tube and gas distribution device configurations (Figures 7a and 7b), the WF_6 concentration decreases from approximately 0.25 at the inlet to 0.15 at the exhaust. In the optimized configuration featuring both a distribution device and a flow baffle (Figure 7c), the inlet concentration remains at 0.25, but the outlet concentration drops further to 0.12. This significantly lower outlet concentration demonstrates a more complete consumption of the precursor, confirming a higher WF_6 utilization efficiency in the final design.

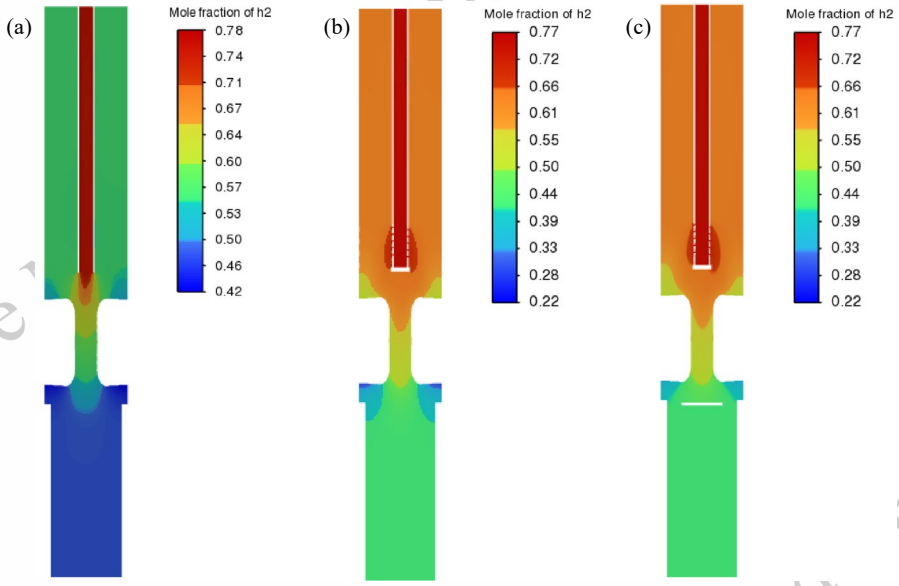

Figure 6. Contour Plots of H_2 Mole Fraction Distribution in Deposition Chambers with Different Structures

(a) H_2 mole fraction contour plot of the straight-tube inlet deposition chamber; (b) H_2 mole fraction contour plot of the deposition chamber with a gas distribution device; (c) H_2 mole fraction contour plot of the deposition chamber with both a gas distribution device and a flow baffle

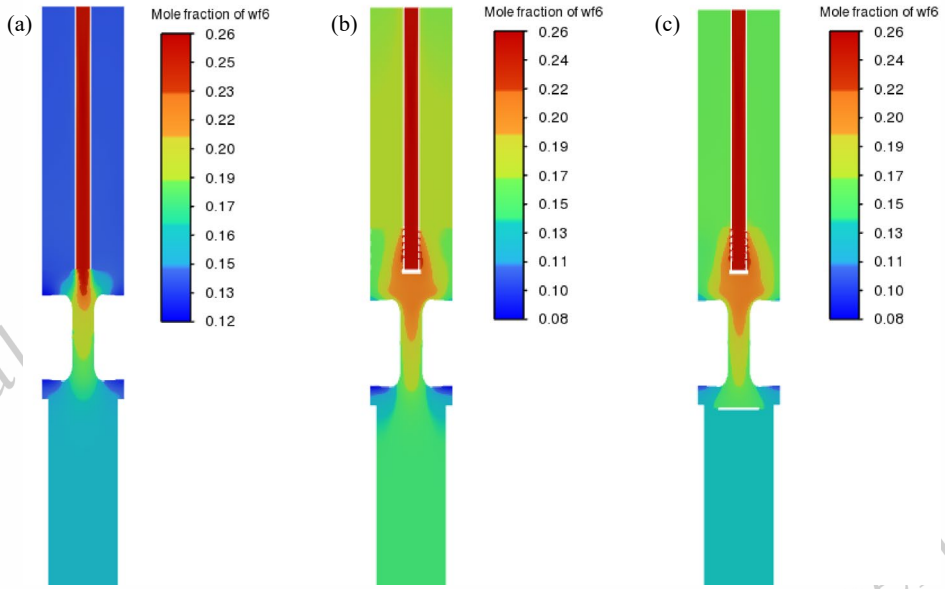

Figure 7. Contour Plots of WF_6 Mole Fraction Distribution in Deposition Chambers with Different Structures

(a) WF_6 mole fraction contour plot of the straight-tube inlet deposition chamber; (b) WF_6 mole fraction contour plot of the deposition chamber with a gas distribution device; (c) WF_6 mole fraction contour plot of the deposition chamber with both a gas distribution device and a flow baffle

3.4 Distribution of Tungsten Deposition Rate on the Throat Liner Surface

Figure 8 presents the tungsten deposition rate profiles along the throat liner cross-section for the three reactor configurations, with the positive x-axis corresponding to the gas flow direction. The deposition rate in the straight-tube inlet chamber is markedly lower than in the configurations employing gas distribution devices. This is attributed to insufficient preheating of the reaction gases in the straight-tube design, which results in a lower substrate temperature and consequently suppresses the deposition reaction kinetics.

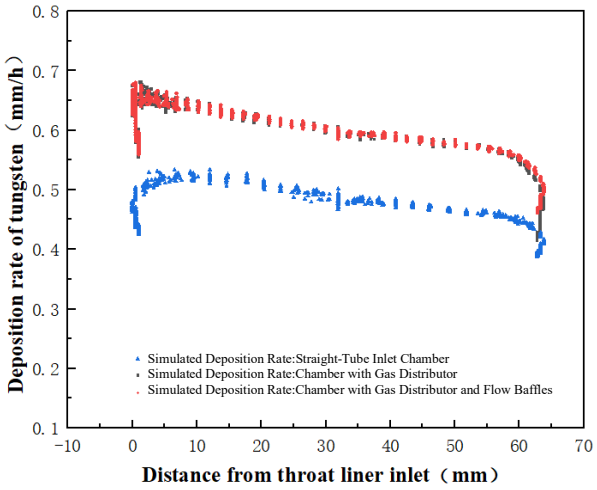

Figure 8. Tungsten Deposition Rates on the Throat Liner Surface in Three Different Deposition Chambers

In the upstream region, the deposition rates for chambers with a gas distribution device (both with and without a baffle) are comparable. A significant divergence, however, occurs downstream, where the configuration incorporating the flow baffle exhibits a markedly higher deposition rate. This demonstrates that the combined use of a gas distribution device and a flow baffle enhances process homogeneity by improving the distribution of reactant gases and the thermal profile within the liner cavity.

3.5 Verification Experiment

To validate the simulation results, tungsten coatings were deposited using the two highest-performing reactor configurations identified by the CFD analysis: one with a gas distribution device and the other incorporating both a distribution device and a flow baffle. Figure 9 shows the actual deposition reaction chamber. Figure 9(a) presents the assembled experimental apparatus, including the heating system, gas inlet system, reaction chamber, and other components. Figure 9(b) shows the reaction chamber equipped with thermocouples for temperature measurement. Figures 9(c) and 9(d) display photographs of the gas distribution device and the flow baffle, respectively. This deposition device can operate stably for more than 48 hours.

Figure 10 presents a comparative analysis of the simulated and experimentally measured deposition rates, alongside cross-sectional morphologies of the tungsten coatings, for the reactor configurations with a gas distribution device and with both a device and a flow baffle. In the current study, the simulated deposition rates consistently overestimate the experimental measurements. This deviation arises from the fact that in the simulation of the deposition experiment, we only ap-plied the chemical vapor deposition reaction on the inner surface of the throat liner. In actual deposition, however, deposition reactions also occur on the walls of the cylindrical reaction chamber, the gas distribution device, and other surfaces. These reactions consume the reactants in advance, resulting in a higher simulated deposition rate than the actual one. To align the model with empirical data, the simulated rates were adjusted using a correction factor of 0.8. The coatings exhibit uniform adhesion to the C/C substrate and are macroscopically defect-free, devoid of pores, cracks, or protrusions. In the range of 0–50 mm, the deposition rates in both reaction chambers are approximately 0.6 mm/h. It is in good agreement with the revised simulated deposition rate. Critically, the experimental data con-firm the simulated trend: the deposition rate decreases along the contour of the throat liner in the flow direction. As can be seen from Figure 10, after installing the flow baffle, the tungsten deposition rate is significantly improved in the region beyond 50 mm. Specifically, it increases from the original 0.4 mm/h to 0.5 mm/h at 55 mm, and at 60 mm, the tungsten deposition rate is raised from approximately 0 to 0.3 mm/h. The magnitude of this decrease is significantly attenuated in the configuration incorporating the flow baffle. This result validates that the flow baffle effectively mitigates the downstream depletion of reactants, leading to a more uniform deposition profile.

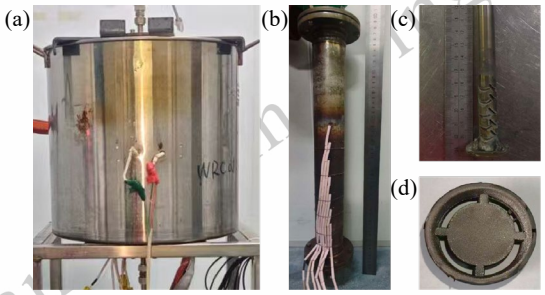

Figure 9. actual deposition reaction chamber

(a) the assembled experimental apparatus;(b) the reaction chamber equipped with thermocouples;(c) the gas distribution device;(d) the flow baffle

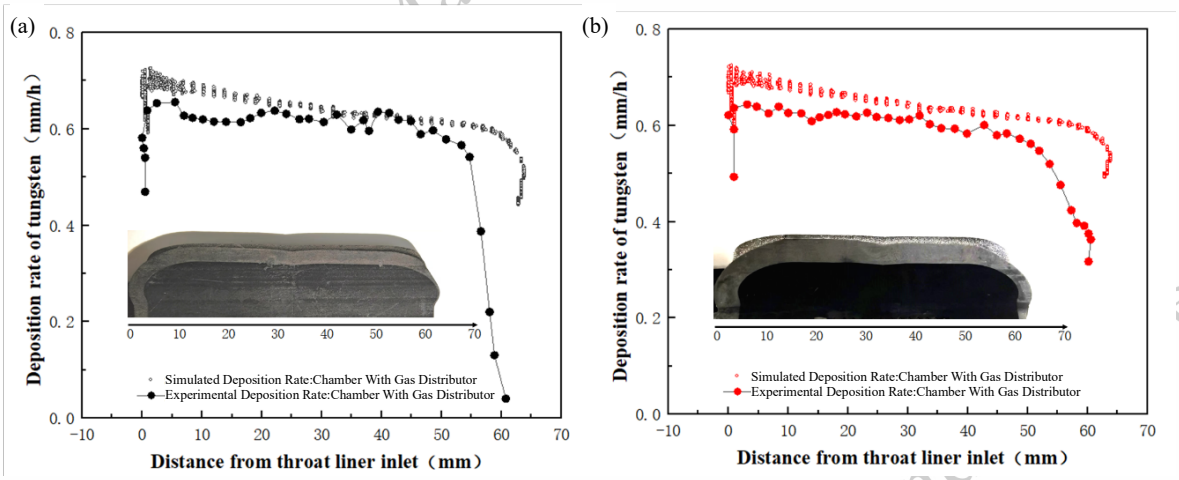

Figure 10. Physical Tungsten Coating Samples in Two Deposition Chambers and Comparison of Actual vs. Simulated Deposition Rates

(a) Tungsten coatings, simulated tungsten deposition rate, and actual tungsten deposition rate in the chamber with a gas distribution device;

(b) Tungsten coatings, simulated tungsten deposition rate, and actual tungsten deposition rate in the chamber with both a gas distribution device and a flow baffle

The deviation between simulated and experimental deposition rates in the lower liner region is attributed to a phenome-non not included in the CFD model: deposition of tungsten on the flow baffle itself. This competing reaction consumes re-actant species, reducing the concentration of reactant gas at the substrate surface and leading to the observed sup-pression of the local deposition rate.

Received date:
Foundation item:
Corresponding author: Tan Chengwen, Ph.D.,Professor,School of Materials Science and Engineering, Beijing Institute of Technology, Beijing 100081, China, E-mail: tanchengwen@bit.edu.cn;Yu Xiaodong, Ph.D., Professor, School of Materials Science and Engineering, Beijing Institute of Technology, Beijing 100081, China, E-mail: yuxd@bit.edu.cn.

Figure 11 presents metallographic micrographs of the resulting CVD tungsten coatings, showing the microstructures at (a) the outlet region and (b) a planar surface region of the throat liner. The deposited tungsten exhibits a polycrystalline micro-structure, growing primarily in the direction normal to the substrate surface. The coating morphology can be delineated into two distinct zones along the growth direction: Zone A (Competitive Growth Zone): Located adjacent to the substrate, this region is characterized by initial nucleation and competitive growth. The gradual increase in grain width indicates a growth competition where preferentially oriented grains outcompete and eliminate their neighbors. Zone B (Columnar Grain Zone): In this upper region, competitive growth ceases. The grains exhibit a stable, columnar morphology with minimal width variation, indicating a transition to self-similar growth where the dominant crystal orientations have prevailed.

The density of the tungsten coating was measured using the Archimedes displacement method, and it reached 19.17g/cm^3, which is close to the theoretical density of tungsten, which is 19.25g/cm^3. Figure 12 shows the surface morphologies of the top surface and cross-section of the CVD tungsten coating. As can be seen from Figure 12(a), the surface of the tungsten coating is composed of numerous "pyramids", which represent the outermost exposed tops of the CVD tungsten grains. Figure 12(b) indicates that the CVDW coating is dense and essentially free of internal defects. As illustrated in Figure 12(c), the deposited tungsten fills the pores of the substrate and forms an anchoring bond with the substrate.

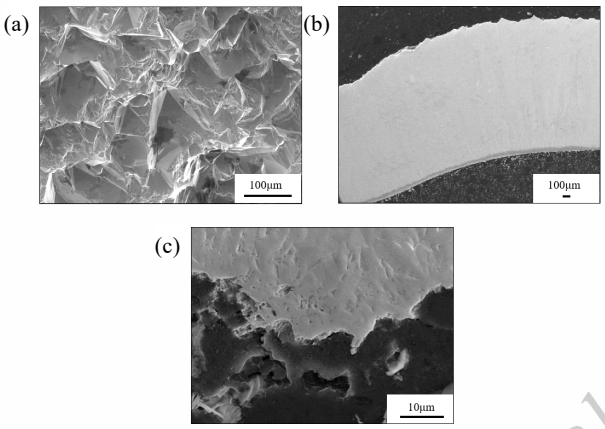

Figure 12. Morphology of the CVD tungsten coating

(a)Morphology of the top surface of the CVD tungsten coating;(b)Morphology of cross-section of the CVD tungsten coating;(c)Morphology of the interface between tungsten coating and substrate

To characterize the bonding strength between the tungsten coating and the C/C matrix, cylindrical samples with a diameter of 8 mm were cut from the throat liner for tensile testing. Figure 13 shows the photographs of the samples before and after the tensile test. A large number of matrix carbon particles and carbon fibers adhere to the fracture surface, indicating that an excellent bonding between the coating and the substrate has been achieved. The fracture occurs mainly inside the substrate. In fact, since C/C composite is a porous material with multi-scale interfaces inside, the bonding strength between these internal interfaces is lower than that between the coating and the substrate. Consequently, the failure during tensile testing initiates preferentially within the substrate. The results show that the tensile strength between the coating and the matrix is approximately 4.6 MPa.

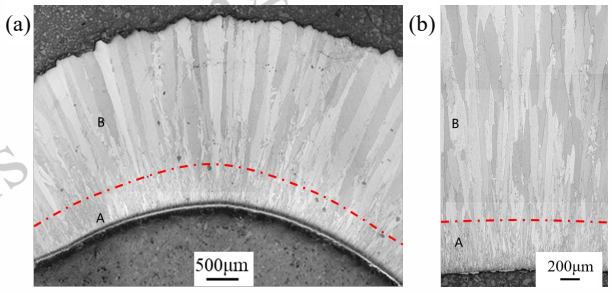

Figure 11. Metallographic Microstructures of CVD-Deposited Tungsten Coating

(a) Metallo-graphic microstructure of the tungsten coating at the outlet region of the throat liner;(b) Metallographic microstructure of the tungsten coating at the planar surface region of the throat liner

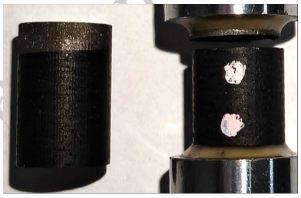

Figure 13. Photo of the samples before and after the tensile test

4 Conclusions

This study integrated CFD with experimental validation to systematically optimize CVD reactor for depositing tungsten coatings on rocket engine throat liners. The findings demonstrate that a straight-tube inlet configuration generates vortices above the liner, resulting in non-uniform temperature and reactant concentration fields. Replacing this with a lateral gas distribution device enhances flow distribution and gas preheating, mitigating temperature gradients; however, it fails to prevent a significant downstream decrease in the deposition rate. The final, optimized design—incorporating both a gas distribution device and a flow baffle—successfully eliminates vortices by promoting radial flow diffusion. This creates a uniform flow field and stable thermal environment, which ensures consistent reaction conditions. Finally, a tungsten coating with a density of 19.17g/cm^3 was obtained, and the tungsten coating bonded well with the substrate.

By adapting a low-pressure CVD model for atmospheric-pressure operation, this work has successfully addressed the critical challenge of depositing uniform, high-quality tungsten coatings on complex-shaped components. The optimization strategy and validated model presented herein provide a robust framework for the design of high-performance CVD systems for advanced aerospace applications.

References

1. Donchev A, Mengis L, Couret A et al. *Intermetallics* **2021,** *139*, 107270.
2. Zhang S, Wang K, Hu J et al. *Rare Metal Materials and Engineering* **2021,** *50* (11), 4073-4078.
3. Popov O; Vishnyakov V. *Journal of Nuclear Materials* **2025,** *611*, 155817.
4. Weerasinghe A, Wirth B D; Maroudas D. *Journal of Applied Physics* **2022,** *132* (18).
5. Škoro G P, Bennett J R J, Edgecock T R et al. *Journal of Nuclear Materials* **2012,** *426* (1), 45-51.
6. Lee D, Umer M A, Ryu H J et al. *International Journal of Refractory Metals and Hard Materials* **2014,** *43*, 89-93.
7. Greuner H, Bolt H, Böswirth B et al. *Fusion Engineering and Design* **2005,** *75-79*, 333-338.
8. Zhan J, Wang H, Wang H et al. *International Journal of Refractory Metals and Hard Materials* **2024,** *123*, 106773.
9. Quesnel E, Pauleau Y, Monge-Cadet P et al. *Surface and Coatings Technology* **1993,** *62* (1), 474-479.
10. Lian Y, Liu X, Cheng Z et al. *Journal of Nuclear Materials* **2014,** *455* (1), 371-375.
11. Pauleau Y; Lami P. *Journal of The Electrochemical Society* **1985,** *132* (11), 2779.
12. Lv Y, Song J, Lian Y et al. *Journal of Nuclear Materials* **2015,** *457*, 317-323.
13. Zhang M, Hu C, Cai H et al. *Rare Metal Materials and Engineering* **2022,** *51* (8), 2830-2838.
14. Zhou Z, Tao C, Chen B et al. *Advanced Engineering Materials* **2023,** *25* (12), 2201781.
15. Lian Y, Feng F, Wang J et al. *Journal of Nuclear Materials* **2019,** *513*, 241-250.
16. Bryant W A. *Journal of The Electrochemical Society* **1978,** *125* (9), 1534.
17. Lakhotkin Y V. *Protection of Metals* **2008,** *44* (4), 319-332.
18. Lakhotkin Y V, Kuz'min V P, Rybkina T I et al. *Inorganic Materials* **2000,** *36* (5), 454-457.
19. Arora R; Pollard R *Journal of The Electrochemical Society* **1991,** *138* (5), 1523.
20. Kleijn C R, Dorsman R, Kuijlaars K J et al. *Journal of Crystal Growth* **2007,** *303* (1), 362-380.
21. Raumann L, Coenen J W, Riesch J et al. *Surface and Coatings Technology* **2020,** *381*, 124745.
22. Raumann L, Coenen J W, Riesch J et al. *Metals* **2021,** *11* (7).
23. Raumann L, Coenen J W, Riesch J et al. *Nuclear Materials and Energy* **2021,** *28*, 101048.
24. Wang Y, Peng L, Zhao Y et al. *ACS Omega* **2025,** *10* (18), 18571-18582.

CVD 法在喉衬上制备均匀致密钨涂层的工艺优化

谢铮[1]，汪龙龙[1]，谭成文[1,2]，于晓东[1,2]，宁先进[1]

(1. 北京理工大学 材料学院，北京 100081)

(2. 海朴精密材料（苏州）有限责任公司，江苏苏州 215211)

摘　要：钨优异独特的物理化学性能，使其成为适用于火箭领域的理想材料。化学气相沉积（CVD）技术能够在复杂构件（如火箭发动机喉衬）表面制备均匀的钨涂层，应用前景广阔。本研究对已建立的钨低压化学气相沉积模型进行改进，使其可在常压条件下于火箭发动机喉衬表面沉积高性能涂层。研究分析了三种不同反应器结构——直管进气反应室、加装布气装置反应室、加装布气装置与引流板反应室，以及结构对反应室内流动特性、温度场、组分浓度及沉积反应的影响。数值模拟与实验结果表明，采用布气装置与引流板相结合的反应室可通过增强气体径向扩散，消除反应室喉衬处的涡流，从而显著提升流场均匀性。该优化设计不仅提高了喉衬构件表面沉积速率的均匀性，还小幅提升了六氟化钨的利用效率。本研究为高均匀性钨涂层化学气相沉积系统的设计提供了理论基础，同时为其工程化应用提供了可行方案。

关键词：CVD; 钨; CFD; Fluent

作者简介：谢铮，男，2002 年生，硕士生，北京理工大学材料学院，北京 100081， E-mail: 3120231005@bit.edu.cn

Rare Metal Materials and Engineering
Rare Metal Materials and Engineering